LASER INTERFEROMETER GRAVITATIONAL WAVE OBSERVATORY
- LIGO -
CALIFORNIA INSTITUTE OF TECHNOLOGY
MASSACHUSETTS INSTITUTE OF TECHNOLOGY

Technical Note	LIGO-T2200160–v1	2022/07/27

Mode Matching for Triangular Ring Cavity

Peter Carney, Shruti Jose Maliakal, Aaron Markowitz, Rana Adhikari

California Institute of Technology
LIGO Project, MS 18-34
Pasadena, CA 91125
Phone (626) 395-2129
Fax (626) 304-9834
E-mail: info@ligo.caltech.edu

Massachusetts Institute of Technology
LIGO Project, Room NW22-295
Cambridge, MA 02139
Phone (617) 253-4824
Fax (617) 253-7014
E-mail: info@ligo.mit.edu

LIGO Hanford Observatory
Route 10, Mile Marker 2
Richland, WA 99352
Phone (509) 372-8106
Fax (509) 372-8137
E-mail: info@ligo.caltech.edu

LIGO Livingston Observatory
19100 LIGO Lane
Livingston, LA 70754
Phone (225) 686-3100
Fax (225) 686-7189
E-mail: info@ligo.caltech.edu

http://www.ligo.caltech.edu/

1 Introduction

The triangular ring cavities in the Phase Sensitive Optomechanical Amplifier (PSOMA) implement two lenses prior to the input mirror which serve as mode matching lenses to help focus our beam into the cavities. Focusing the beam to the proper size so that it matches the cavity eigenmode will create resonance within the cavity, and be considered mode matched. However, in the process of analytical calculation, the resonances we expect are not the resonances we find in practice, which leads us to believe that we are mode mismatched. There are various approaches to try and solve this problem. Two possible solutions could be creating a model using a thick lens, and considering the lens aberrations. If our models show non-negligable change in upon use of thick lenses and account of aberrations, then these may be factors to consider in future tabletop experiments.

2 Mode Matching Tolerances

Before we begin approximating with a thick lens, we first look at the tolerance the tabletop cavity has to changes in positioning and focal lengths of the lenses. It is key to note here, that we start off by simplifying our triangular cavity into a Fabry-Perot cavity, in which the two end mirrors can be approximated as a single plano mirror at the end of the beam path, as seen in Figure 1 on the following page. The round trip propegation that would occur in a three mirror cavity is used to set the distance of our two mirror model. In this case, the length of the two mirror cavity is half the propegation distance of our ring cavity.

Let us first examine the tolerance of our ring cavity in its current set up. In Figure 2, it can be seen that in both the contour and heat map, we vary both lens 1 and 2 around their respective resonance positions. One thing to note here is the major effects on resonance by the movement of lens 2. It is not hard to convince yourself that this is the case, since lens 2 is directly in front of the first mirror of the cavity, giving it significant control of the beam width entering the cavity.

We then transition from a two mirror model to a ring cavity model to determine accuracy and effectivness the mode matching. The different models do not make a significant difference in the tolerances to change in lens positions, as seen in Figure 3. Again, it can be shown that the second lens allows less room for movement as the first lens. This will be useful to know in our attempts in solving the discrepency in mode matching that we find.

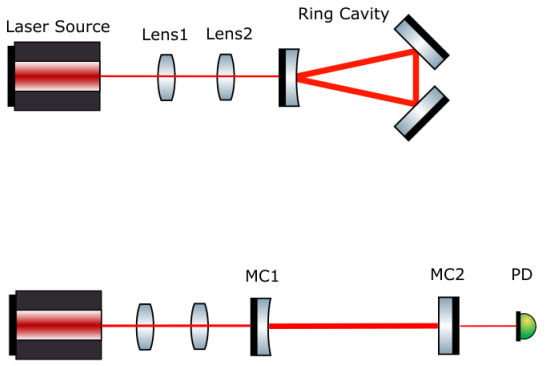

Figure 1: Visual of approximation being made with the combination of lenses and mirrors. Note the pd at the end of the cavity, used for sensing transmitted power. When cavity on resonance, the power transmitted will be at a maximum.

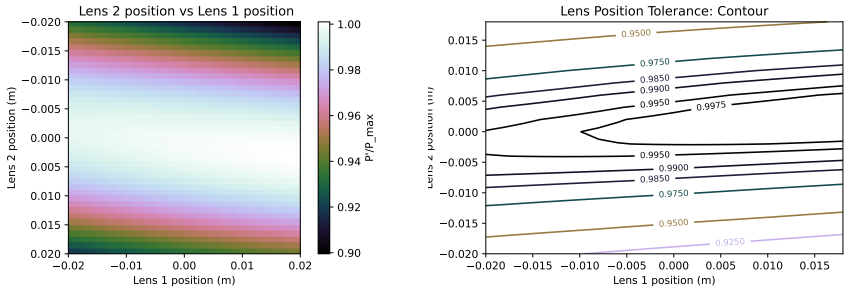

Figure 2: Two Mirror Model (a) A heat map of the power transmitted at varying lens positions relative to the maximum power (which is resonance) of our two mirror model. (b) Contour map of (a). Our current set up has dimesions: lens 1 = 0.0617m from laser, 0.10322m focal length, lens 2 = 0.3502m from laser, 0.15482m focal length.

We then transition from a two mirror model to a ring cavity model to determine accuracy and effectivness the mode matching. The different models do not make a significant difference in the tolerances to change in lens positions, as seen in Figure 3. Again, it can be shown that the second lens allows less room for movement as the first lens. This will be useful to know in our attempts in solving the discrepency in mode matching that we find.

Another interesting plot to consider is a comparison of different combinations of previously tested mode matching solutions. Each combination has a different set of focal lengths and lens positions. Ideally, we want to use the configuration that has the most tolerance to changes in position. Figure 4 shows a similar contour as seen in the previous two figures, yet for this one, we consider multiple solutions of mode matching. If need be, we can pick from one of these solutions to help give us more room for forgiveness in our attempts to mode match the cavity.

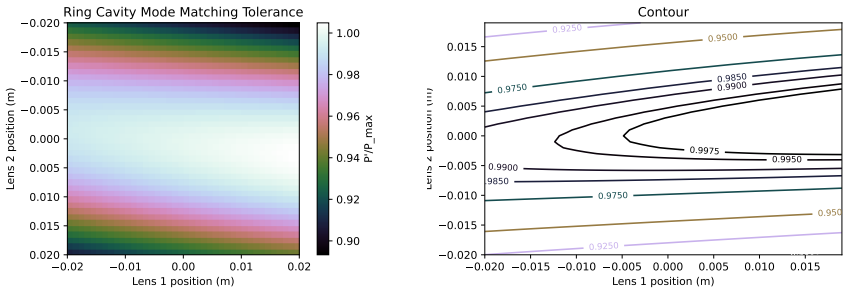

Figure 3: Three Mirror Model (a) A heat map of the power transmitted at varying lens positions relative to the maximum power (which is resonance) of our three mirror model. (b) Contour map of (a). Our current set up has dimesions: lens 1 = 0.0617m from laser, 0.10322m focal length, lens 2 = 0.3502m from laser, 0.15482m focal length.

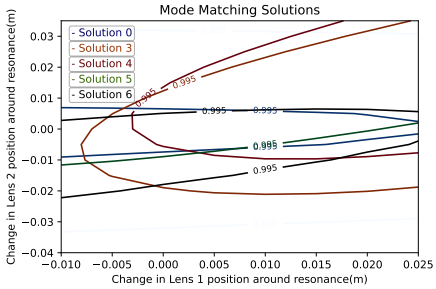

Figure 4: Here we have a comparison of different solutions of lens positions and focal lengths. The area within each contour represents the area in which the cavity has 99.5 percent resonance or more.

3 Thick Lenses

A begining model of thick lenses is already in progress. First, a thin lens ABCD matrix calculation for a laser propegating through two lenses and a two mirror cavity has been made, and tested for accuracy. Though the thick lens ABCD calculation still has some debugging to do at its current stage, it is not difficult to implement a thick lens.

Figure 5 shows us how a beam propegates through such a lens. The initial radius of curvature acts as a thin lens, then the middle of the lens carries the beam through a medium with some index of refraction, and then the back surface of the lens acts as another thin lens. The difference in focal length can cause us to fall out of resonance on our cavity. For calculation purposes, instead of having a matrix

$$\begin{pmatrix} 1 & 0 \\ \frac{-1}{f} & 1 \end{pmatrix}$$

We end up with the matrices:

$$\begin{pmatrix} 1 & 0 \\ \frac{n_2-n_1}{R_2} & 1 \end{pmatrix} \begin{pmatrix} 1 & \mathrm{d} \\ 0 & 1 \end{pmatrix} \begin{pmatrix} 1 & 0 \\ \frac{n_1-n_2}{R_1} & 1 \end{pmatrix}$$

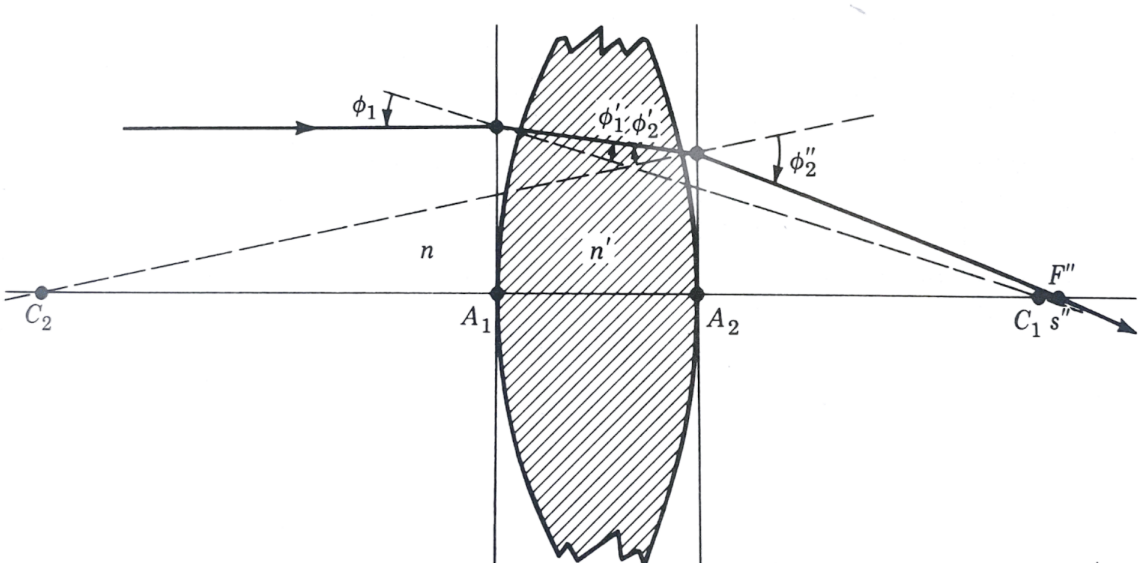

Figure 5: Diagram of a ray propegates through a thick lens. Notice the small change focal length of the lens, C_1 to F''

Where d is the thickness of the lens, R_1 and R_2 are the radii of curvature of the front and back ends respectively, and n_1 and n_2 are the indices of refraction of the air and mirror respectively.

4 Lens Aberrations and Third Order Theory

Another issue that may be contributing to this discrepency in our mode matching are lens aberrations. Lens aberrations can come in a variety of different forms, and each can create higher order modes that do not resonate in the cavity. This section is to provide a basic introduction to lens aberrations by using ray tracing figures and paraxial beams. In the next section, lens aberrations with Gaussian beams will be discussed.

Lens aberrations may be due to the curvature of the lens not being completely accurate for image focusing. As a result, the image can become blurry, and we can see varying focal points for varying rays of light. This can be seen in Figure 6a, as there are multiple points along the propegation axis where the light comes into focus.

One key thing to note is that the higher up the beam comes through the lens, the larger the distance is between its focusing point, s_h', and the paraxial focal point f'. Under ideal circumstances, the distance of the image once passing through a lens can be modeled with only a first order approximation of sine, since the angle θ shown in Fig 6b is small.

However, if we picture this point source as a beam waist of gaussian beam, we see that as the beam diverges further, it passes through the lens with greater width, causing our value

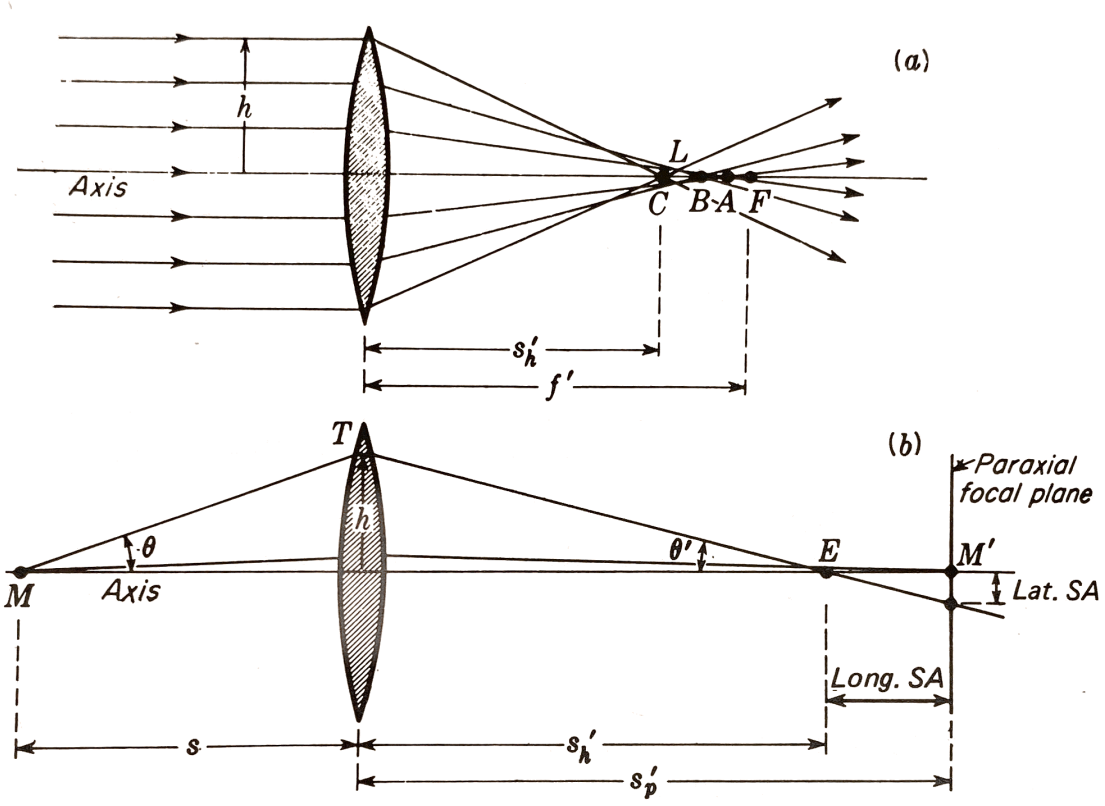

Figure 6: From *Fundamentals of Optics* Francis A. Jenkins and Harvey E. White. Chp. 9 (a) Diagram of how lens aberrations occur, and how they can be perceived. (b) Notice here the Longitudinal Spherical Aberrations (Long. SA) and Latitudinal Spherical Aberrations (Lat. SA), which come in to play in the beam being misaligned within the cavity.

of h and θ in this figure to become large enough to need third order approximation of the expantion of sine.

$$sin(\theta) \approx \theta - \frac{\theta^3}{3!} \tag{1}$$

Now in reality, θ for our table top experiment will still be very small, yet it may be useful to still use third order approximation anyways considering how precise we need our cavity to be. When using third order to solve for the image length, we end up with:

$$\frac{n}{s} + \frac{n'}{s'_h} = \frac{n'-n}{r} + \left[\frac{h^2 n^2 r}{2f'n'}\left(\frac{1}{s}+\frac{1}{r}\right)^2\left(\frac{1}{r}+\frac{n'-n}{ns}\right)\right] \tag{2}$$

We see that as h increases, we get a larger right hand side of the equation, meaning that s'_h gets smaller on the left side to compensate, making the lens aberration greater. This tells us that if the laser beam is wide enough upon entering the lens, then lens aberrations may cause higher order modes in the cavity that do not align to the resonance conditions we originally plan for.

5 Analyzing Aberrations

All the models we have considered are rays. It is difficult to create a numerical analysis of lens aberrations given in the pervious section with Gaussian beams, since they diverge with curvature. To account for this, we can shift the focus of the project analyze the beam intensity distribution after propegating through optical surfaces.

Doing this will require using a Gaussian beam field equation, and using a mode coupling formula.

The general form of a Gaussian beam is

$$E(x,y,z) = E_0 e^{-i(\omega t - kz)} \frac{\omega_0}{\omega(z)} e^{\left(-ik\frac{x^2+y^2}{2R(z)} - \frac{x^2+y^2}{\omega(z)}\right)} e^{i\psi(z)} \tag{3}$$

Where k is the wave number, z is the position on the propegation axis, $R(z)$ is the Gaussian beam radius of curvature at z, ω_0 is the beam waist, $\omega(z)$ is the beam width at z, and psi is the Gouy phase. We can define u as:

$$u(x,y,z) = \sqrt{\frac{2}{\pi}} \frac{1}{\omega(z)} e^{\left(-ik\frac{x^2+y^2}{2R(z)} - \frac{x^2+y^2}{\omega(z)}\right)} e^{i\psi(z)} \tag{4}$$

Which represents the spatial properties of the beam. The equation, $u(x,y,z)$ is a solution to the paraxial wave. However, when a beam is not perfectly aligned or mode matched within the cavity, there can be higher order modes that propegate in the cavity.

These higher order modes are families/sets of solutions to the paraxial wave equation. The two types of modes possible are Hermite-Gauss (HG) modes, and Laguerre-Gauss (LG) modes. Currently, my research has focused only on HG modes, which have the form.

$$u_{nm} = \left(2^{n+m-1} n! m! \pi\right)^{-1} \frac{1}{\omega(z)} e^{(i(n+m+1)\psi(z))} H_n \frac{\sqrt{2}x}{\omega(z)} H_m \frac{\sqrt{2}y}{\omega(z)} e^{\left(-ik\frac{x^2+y^2}{2R(z)} - \frac{x^2+y^2}{\omega(z)}\right)} \tag{5}$$

In which the polynomials H_n and H_m have the general form:

$$H_0 = 1$$
$$H_1 = 2x$$
$$H_2 = 4x^2 - 2$$
$$H_3 = 8x^3 - 12x$$

After a beam has propegated, we can express it with a summation of all higher order modes:

$$u(x, y, z) = \Sigma c_{nm} u_{nm}(x, y, z) \tag{6}$$

In which c_{nm} is a coefficient of amplitude and phase of each mode.

Since each all HG u_{nm} represent an infinite set of orthonormal basis vectors (once normalized), inner product of the complex conjugate, which yeilds:

$$\iint_{-\infty}^{\infty} u_{nm} u^*_{n'm'} dx dy = \delta_{nn'} \delta_{mm'} \tag{7}$$

This property allows us to find coupling coefficients between different modes.

As the beam propegates through an optical element, perturbations/imperfections in the surface of the optic can cause what was once a 00 mode to spill in to higher order modes, and have the resulting beam become a superposition of these modes. This is a lens aberration for a Gaussian beam, since the width of the beam at the focal point is not the width to be expected. The amplitude of each mode is determined by the coupling coefficients.

The surface of an optic (in this case it is beneficial to use a lens), is modeled by an equation $Z(x, y)$ which describes the height Z of an optic as a function of x and y, which run perpendicular to the axis of beam propegation.

Using this, we can construct a formula to determine the coupling coefficients:

$$c_{nm} = \iint_{-\infty}^{\infty} u_{nm} u^*_{n'm'} e^{(2ikZ(x,y))} dx dy \tag{8}$$

After implementing this into code, and constructing a model lens surface of arbitrary curvature, I generated an intensity distribution map of a Gaussian beam before entering the lens,

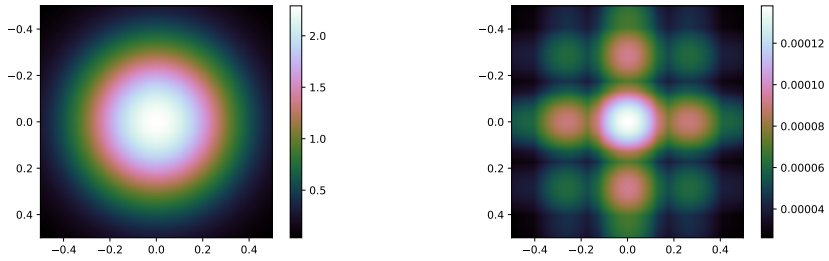

Figure 7: (a) An intensity distribution of a 00 order Gaussian beam as a function of positions x and y. (b) Intensity distribution of a superposition of higher order HG Gaussian beams with coupling coefficients.

and after entering the lens. Though the results are still a work in progress, the overall idea that the post-lens map is a superposition of modes can easily be seen in figure 7b.

It is clear that there is no clar Gaussian beam distribution, even with a sum of all of these modes. This is (likely) the affect of a lens aberration on a Gaussian beam. These types of modes can create a problem with resonances in not just the PSOMA cavity, but in the LIGO interferometer as well.

6 Next Steps

Once we get a better idea of how to run this beam simulation, the next immediate steps will be to test different Z functions to see how different surfaces affect beams. The goal will be to try and model something that gives us a near spherical surface towards the center of the optic, but then becomes less and less spherical as we get closer to the edge.

Once that is done, we can then move into modeling these surfaces within the analytical simulation to try and create a q factor that will match the PSOMA ring cavity eigenmode. Once we have determined a surface that works, we can then do a mode matching tolerance with it, by varying its respective position, just as done in the beginning sections of this paper.

Another direction that may also be possible to go into is using actual LIGO mirror surface maps to try and model how a Gaussian beam actually propegates through it, and determine whether or not aberrations should be taken into account.

References

[1] Jenkins A Francis White E. Harvey, *Fundamentals of Optics* McGraw-Hill Inc. 1957.

[2] Burch JM Gerrard A, *Introduction to Matrix Method in Optics* Dover, 1994.

[3] Kenneth Strain Andreas Freise Charlotte Bond Daniel Brown, *Interferometer Techniques for Gravitational-Wave Detection* Physical Review (2015)

[4] Yuntao Bai Gautam Venugopalan Kevin Kuns Christopher Wipf Aaron Markowitz Andrew R. Wade Yanbei Chen and Rana X Adhikari, *A phase-sensitive optomechanical amplifier for quantum noise reduction in laser interferometers*. Physical Review (2020).